Green Chemistry

PAPER

View Article Online
View Journal

Cite this: DOI: 10.1039/d5gc02382c

Beyond bubbles: greener flow-based electroanalysis by an air-driven carrier

Tayná Silva Bernardino Barros,[a] Eloise de Lima Osorio,[a] Cláudio Teodoro de Carvalho,[a] Raphael Rodrigues,[a] Lucio Angnes [b] and Magno Aparecido Gonçalves Trindade *[a,c]

Received 13th May 2025,
Accepted 3rd August 2025

DOI: 10.1039/d5gc02382c

rsc.li/greenchem

To minimize environmental issues and operational costs, using air to manipulate analyte/sample movement within milli/micro-sized channels can be a fascinating feature for flow-based electrochemical systems. However, maintaining uniform flow and undisturbed measurements during air bubble formation exhibits a considerable challenge. Here, we present a dual-mode electrochemical detection system that enables the use of air-driven carriers for controlling discrete electrolytic analyte solution injections, ensuring that transient signals remain unaffected by air bubble formation or when dealing with real-world samples. The proposed system effectively addresses critical limitations, such as air bubble interference, analyte dilution issues, contamination risks at the working electrode, and channel clogging, thereby minimizing maintenance. Performance evaluations validate the system's robustness and the reproducibility of measurements, ensuring the maintenance of analyte concentration during transport within the channel. Additionally, it demonstrates superior performance compared to traditional liquid-flow methods by reducing sample volume, minimizing waste generation, and lowering operational costs. Thus, this paper highlights the advantages of air-driven solutions for controlled analyte/sample injections, emphasizing their potential for more environmentally friendly flow-based electroanalysis.

Green foundation

This work advances green chemistry by introducing an air-driven flow system for electroanalysis, reducing reliance on liquid carriers, minimizing waste generation, and lowering operational costs compared to traditional liquid-flow electroanalysis.

This achievement aligns with the green chemistry principle of waste reduction by using an airflow carrier to drive the samples through the system, reducing the need for liquid carriers. The air-driven system allows for smaller sample injection volumes, leading to less waste compared to liquid-flow methods that require continuous pumping of a liquid mobile phase and larger injection volumes.

Further research could make this work greener by exploring alternative materials for the electroanalytical platform to enhance its sustainability and reduce the use of acetone in the fabrication process.

1. Introduction

The increasing emphasis on sustainability and environmental consciousness in modern scientific research has driven the demand for greener analytical techniques.[1,2] Flow-based methods have been crucial in addressing this need, as well as the requirement for rapid chemical analysis, providing precise and efficient methods for a wide range of applications.[1,3–5] Flow injection analysis (FIA), a well-established technique for automated and rapid chemical analysis, has been a fundamental technique in analytical laboratories for many years.[1] However, the usual FIA systems rely on the use of liquid-flow carriers, which can pose environmental concerns and contribute to operational costs.[5,6]

In recent years, the focus has emerged on creating more eco-friendly analytical procedures that minimize waste and reduce the reliance on hazardous chemicals. Transitioning to microfluidics flow-based methods has been reported to considerably reduce these issues.[5,7] Indeed, their small scale and precise manipulation of fluids offer a promising context for minimizing liquid carriers within hydrodynamic systems. By

[a]Faculdade de Ciências Exatas e Tecnologia, Universidade Federal da Grande Dourados, Rodovia Dourados-Itahum, km 12, 79804-970 Dourados, MS, Brasil. E-mail: magnotrindade@ufgd.edu.br, magnotr@gmail.com
[b]Departamento de Química Fundamental, Instituto de Química, Universidade de São Paulo, Av. Prof. Lineu Prestes, 748-05508-000 São Paulo, SP, Brasil
[c]National Institute for Alternative Technologies of Detection, Toxicological Evaluation and Removal of Micropollutants and Radioactives (INCT-DATREM), Institute of Chemistry, P.O. Box 355, 14800-900 Araraquara, SP, Brasil

exploiting the typical characteristics of microfluidic channels, the development of novel analytical systems that decrease the need for liquid flow (such as supporting electrolyte solutions) while preserving high sensitivity and selectivity becomes achievable.

An interesting strategy for enhancing carrier systems involves using air to drive the analyte or sample within channels. For example, segmented flow analysis (SFA) is a well-established technique that involves introducing air bubbles into a continuous stream of samples as they move through the measurement system, leading to more accurate measurements by reducing the analyte dispersion within the tubing.[8] The flow generated by bubbles has found use in many microfluidic applications, including homogeneous micromixers,[9] pulsatile chemical gradients,[10] acoustic bubble-based micropumps,[11] and multiple actuation technologies induced by microbubbles.[12] However, despite the benefits observed in flow-based applications, challenges associated with bubble formation and its impact on measurement accuracy have limited its widespread use.[5] Light scattering caused by air bubbles during analyte carry presents a significant source of error in detector readings.[6] Moreover, air bubbles within the pumping capillary can interrupt the flow path and lead to pump failure due to circuit disconnection.[13] Undesirable air bubbles pose a challenge to flow dynamics by disrupting fluid flow patterns and mixing within microfluidic devices.[14–16] Integrating electrochemical sensors into air-driven microfluidic systems also presents difficulties in maintaining consistent electrical contact during the presence of bubbles.[17–19] Air bubbles also severely affect electrode performance during electrolysis for hydrogen generation by increasing ohmic resistance through adhesion, decreasing the active surface area, and causing bubble overpotentials.[20–24] Additionally, air bubbles pose challenges in organic electrosynthesis, leading to inconsistent flow rates and areas of high electrical resistance.[25]

The integration of electrochemical detectors with hydrodynamic systems has encouraged the development of affordable materials and miniaturized (milli/micro-sized) flow-based electroanalytical platforms. However, conventional flow-through electroanalysis still frequently relies on the use of a liquid carrier.[16] As such, careful selection and potential degassing of the supporting electrolyte solution are crucial to prevent malfunctions arising from air bubble formation.[17,18] Introducing air into these systems can lead to several operational challenges: (I) air bubbles can impede the smooth movement of the analyte towards the electrode surface, causing variations in the diffusion layer thickness;[26] (II) the presence and movement of bubbles can introduce noise into the electrochemical signal, making it difficult to discern the actual signal from background fluctuations;[17–19] (III) air bubbles can also physically block portions of the electrode surface, effectively diminishing the active area available for electrochemical reactions;[18,26] and (IV) the motion or collapse of air bubbles can generate localized turbulence and pressure fluctuations within the electrochemical cell, impacting the stability of the electrochemical interface and hindering electrical contact.[18,19,27,28] These issues can distort the electrochemical response, often leading to a reduction in the measured peak current, which directly compromises the reproducibility of results.

Indeed, precisely controlling air bubbles to maintain consistent flow without disrupting fluid mechanics or electrochemical measurements remains a significant challenge.[17–19] Recently, we have introduced alternative designs featuring (micro/milli)-sized fluidic channels with the dual-mode electrochemical detectors, offering novel solutions to overcome these challenges.[17–19,27,28] The design features two compartments: an upper chamber holding a static electrolyte solution for the reference or reference/pseudo-reference electrode, and a flow channel for the working and counter electrodes, both of which extend into the upper compartment. This electrochemical detector setup allows for both partially and fully referenced configurations[19] and demonstrates resistance to air bubble effects on the working electrode within the flowing channel. Notably, because the upper chamber is not affected by the presence of air bubbles, it can ensure stable potential measurements between the working and reference/pseudo-reference electrodes, opening new opportunities for flow-based electroanalysis using an air-driven flow carrier.

Despite the significant challenges that airflow poses in conventional microfluidic systems,[16] its manipulation can be controlled for specific analytical applications through well-designed electrochemical detectors. Herein, we introduce a polydimethylsiloxane-based electroanalytical platform that uses air to drive the injected analyte/sample solution without impairing the operation of the electrochemical detector. The electrode configuration was optimized to ensure stability by mitigating the effects of carrier fluctuations, including pulsations from micropipette injections and the presence of air bubbles, which can negatively impact the electrochemically active electrode surfaces. We evaluate the discrete injection of liquid analyte/sample into a continuous air-driven carrier and compare the findings with those obtained using a liquid-flow carrier. This advancement offers a promising alternative to traditional flow injection electroanalysis, making it feasible to develop efficient electroanalytical systems that require minimal electrolyte consumption while ensuring reliable measurements in an environmentally friendly manner.

2. Experimental section

2.1. Chemicals, solutions and sample preparation

A standard stock solution (10.0 mmol L^{-1}) of the redox probe ferrocyanide/ferricyanide ($Fe(CN)_6^{4-}/Fe(CN)_6^{3-}$, Sigma) was diluted in a 50.0 mmol L^{-1} KCl solution (Sigma). Standard stock solutions (10.0 mmol L^{-1}) of salicylic acid (Sigma) were utilized in the proof-of-concept experiments, and the working solutions were prepared daily by dilution with 10.0 mmol L^{-1} Britton–Robinson buffer (B–R) and adjusting their ionic strength with 50.0 mmol L^{-1} KCl solution (Sigma). A 50.0 mmol L^{-1} sulfuric acid solution (Sigma) was used to clean

and activate the platinum-based electrodes in the customized electroanalytical platform. The polydimethylsiloxane (PDMS) elastomer and the cross-linking agent (Sylgard™ 184, Dow Corning) were used to prepare the PDMS-based electroanalytical platform.

River water, groundwater, and lake water were collected from the city of Dourados (Dourados, MS, Brazil) and used for the addition–recovery experiments. Before analysis, the required aliquots were filtered through a 0.45 μm nylon filter disc (Millipore®). The salicylic acid calibration solutions were prepared in the supporting electrolyte solution (B–R buffer at pH 7.0 containing KCl at 50.0 mmol L^{-1}) within a concentration range of 0.50 to 10.0 mmol L^{-1}. The external calibration method was employed for all analytical salicylic acid determinations.

2.2. Instrumentation and experimental setup

A reverse osmosis water purifier (Gehaka®, model OS 10 LTXE) was utilized to obtain deionized water ($R \geq 18.2$ MΩ cm) for the preparation of all working solutions. Voltammetric and chronoamperometric measurements, as well as experimental control, were conducted using a potentiostat/galvanostat (Metrohm®, model PGSTAT101) in conjunction with NOVA 2.1.6 software. A combined glass electrode (Hanna®, model HI 1131B) connected to a digital pH meter (Hanna®, model HI 3221) was used to adjust the required pH values. The mixture of PDMS elastomer and the cross-linking agent was cured using a laboratory drying oven (Ethik® Technology). A digital automatic micropipette (Eppendorf®, model Multipette E3X) and micropipette tips of 500 μL were used to inject discrete volumes (*i.e.*, standards and samples) into the electroanalytical platform system. The air-driven carrier was induced using a syringe pump (KD Scientific, model Legato 210P) with a plastic syringe of 20 mL (Luer Lock model) connected to the outlet of the PDMS-based electroanalytical platform. For the liquid-flow system, the carrier solution was introduced into the channel using the syringe pump along with standard 10 and 20 mL syringes. A vacuum pump (Prismatec, model 131 – Type 2 VC) and a desiccator were used to eliminate bubbles before the curing process of the PDMS/curing agent mixture. Channel dimensions were measured by analyzing optical microscope images obtained with a microscope (model B3 T) coupled to a high-resolution 6.0 MP digital camera (BEL Photonics®). Channel sizes were measured by analyzing the images with AxioVision Rel. 4.8 software, and histograms were created based on an average of 30 measurements.

2.3. Customization of the PDMS-based electroanalytical platform

A customized spiral-configured acrylonitrile butadiene styrene (ABS) channel template was prepared using a 3D printing pen, involving the manual wrapping of extruded ABS filament as detailed in our previous work.[18,28] Briefly, the process involved extruding the ABS filament (1.75 mm)—using the 3D printing pen (MYNT3D, model Super 3D Pen) and a 400 μm nozzle—to create a mold. The modeled ABS-based channel was placed into a plastic box, casting PDMS around this mold, and after curing (overnight), the ABS was selectively removed (with acetone) inside the PDMS to form the channel, as detailed in our earlier work.[18,28] Specific parameters, such as the extrusion diameter, PDMS mixing ratio, and ABS removal conditions, were employed as previously optimized.[18,28]

Through a manual fabrication process, we achieved a circular channel with a mean inner diameter of 632 ± 1 μm (detailed in Fig. S1, SI), and the platform featured electrodes arranged in two different configurations (Fig. 1). This version of the PDMS-based electrochemical system comprises a platform with dimensions of 78 × 28 × 18 mm (length × width × height) and is characterized by an external compartment—with a volume of 120 mm^3—designed for accommodating the pseudo-reference electrode (PRE). This compartment ensures continuous contact with both the working electrode (WE) and counter electrode (CE) extending from the patterned channel. Given the consistent placement of the PRE in the dedicated reservoir, the KCl (50.0 mmol L^{-1}) solution was used as the supporting electrolyte for this compartment. This ensured that the PRE-surface remained clean throughout the voltammetric/chronoamperometric measurements, in addition to enabling more effective control of the potential in both electrochemical cells.

Connections between the main parts (details in Fig. 1) were established using PTFE tubing with a 1000 μm inner diameter. A T-junction way (Fig. 1)—created by a three-way PEEK Tee (1/16″)—was used for connecting the automatic electronic micropipette during discrete sample/analyte injection. The electrochemical cell setup involved a platinum-based wire (0.50 mm diameter) as the working and counter electrodes, both positioned within the flow and stationary paths (Fig. 1). A platinum wire (0.50 mm diameter) was designed to be placed in an external compartment and used as the PRE, ensuring electrical contact with the WE and CE.

2.4. Electrode activation and the proof-of-concept experiments

Before conducting voltammetric or chronoamperometric measurements, the electrode surface was activated according to the protocol detailed in our earlier publications[17,18,27] using the configured experimental setup as shown in Fig. 1. This step comprises cleaning the electrode's surface by recording successive cyclic voltammograms between −0.50 and +1.0 V (30 cycles) at a scan rate of 50 mV s^{-1} in a sulfuric acid solution (50.0 mmol L^{-1}), which was pumped at 0.10 μL s^{-1}. This procedure cleaned and activated the electrode's surface, enabling the enhancement of the electrochemical responses throughout the workday.

Chronoamperometric measurements using the air-driven carrier configuration were performed by injecting the analyte solution into the PDMS-based electroanalytical platform with an automatic micropipette (details in Fig. 1). Simultaneously, a syringe pump operating "in withdrawal mode"—at a flow rate of 1.00 μL s^{-1}—was enough to draw atmospheric airflow into the device and carry the injected analyte/sample through

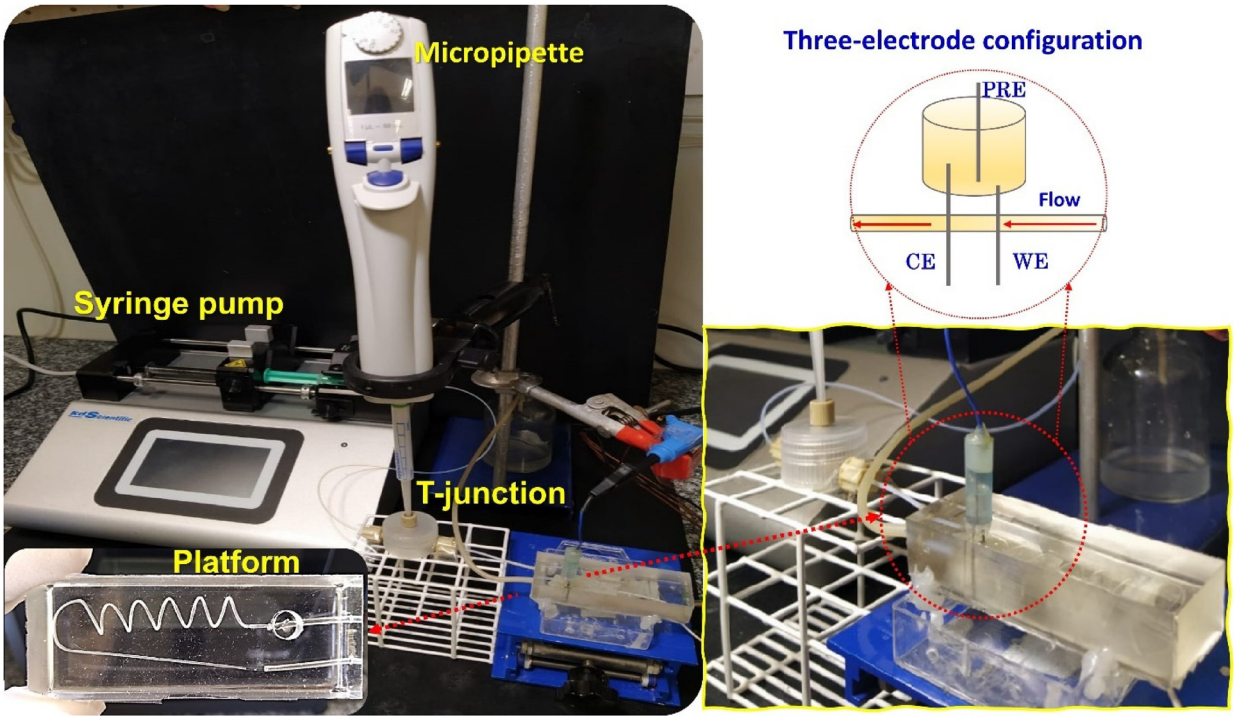

Fig. 1 Schematic representation illustrating the experimental setup: the syringe pump operating in withdrawal mode to drive the injected analyte/sample through the channel, the automated electronic micropipette providing hydrodynamic injection of the analyte/sample, the T-junction system connecting the micropipette, and the PDMS-based electroanalytical platform featuring a coil-shaped channel and an integrated electrochemical cell configuration holding a dual-mode detector system featuring the working electrode (WE), counter electrode (CE) and pseudo-reference electrode (PRE). All electrodes were made from platinum-based wire (0.50 mm diameter).

the channel. To validate the performance of the proposed device, we conducted experiments injecting into the system a redox probe containing a mixture of $Fe(CN)_6^{4-}/Fe(CN)_6^{3-}$ at a total concentration of 10.0 mmol L^{-1} prepared in KCl (at 50.0 mmol L^{-1}) to serve as the supporting electrolyte solution. To determine the optimal operating parameters for this air-driven system, we employed a 2^3 factorial design, which is a systematic approach that enabled us to assess the influence of three key variables: applied potential, airflow rate, and the analyte injected volume.

Following optimization, we evaluated pH adjustments and performed a proof-of-concept application using salicylic acid as the target analyte. To assess the reliability of our air-driven method, a comparative study was conducted using a liquid-flow carrier (B–R buffer solution, 10.0 mmol L^{-1} at pH 7.0 containing 50.0 mmol L^{-1} KCl) as the supporting electrolyte. Whenever possible, both methodologies were tested under identical conditions and parameters to guarantee comparability. The fixed parameters were as follows: flow rate, 15 μL s^{-1}; injection volume, 100 μL; and applied potential, 0.60 V. Spiked samples of river water, groundwater, and lake water, each containing 1.00 mmol L^{-1} salicylic acid, were analyzed, and the results were accurately compared.

The ecological impact of the developed air-driven carrier method was compared to the liquid-flow method using the AGREE metric. This ensures that the electroanalytical protocol was developed following green analytical chemistry principles, aiming to reduce waste and toxic reagents for more ecological and efficient practices in electroanalysis.

3. Results and discussion

3.1. Voltammetric study under stationary configuration

For the stationary configuration, voltammetric studies were performed after filling the flow-based channel with the $Fe(CN)_6^{4-}/Fe(CN)_6^{3-}$ solution and then stopping the pumping before recording measurements. The upper compartment containing the PRE was filled with KCl (at 50.0 mmol L^{-1}), which served as the supporting electrolyte solution. In this partially referenced system, the PRE lacks direct ionic contact with the flowing channel. The background scan (Fig. 2) was decisive in verifying the proper functionality of all electrochemical cell components before introducing the analyte. This step confirmed the absence of significant capacitive and resistive effects, as well as ensured that no redox events are observed, which can otherwise compromise data analysis.

The staircase cyclic voltammogram (Fig. 2) for the redox probe exhibits deviations from the ideal reversible shape, characterized by asymmetry between the anodic and cathodic peaks and a larger-than-expected peak-to-peak separation. While not perfectly ideal, this voltammetric profile still indi-

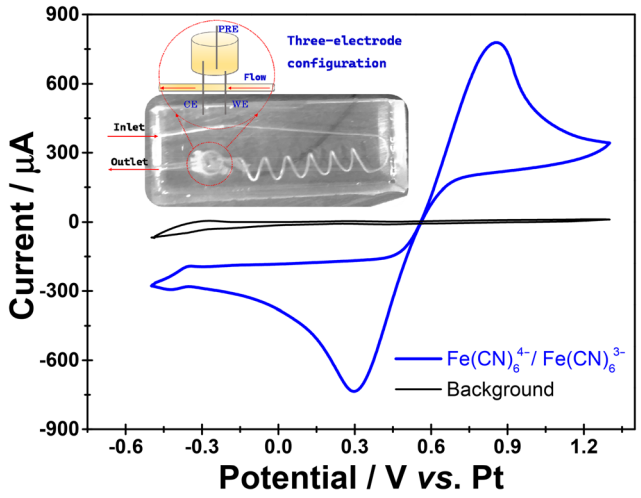

Fig. 2 (Inset) Image illustrating the PDMS-based electroanalytical device with a dual-mode electrochemical detector. Cyclic voltammograms recorded in the absence (background) and presence of potassium ferrocyanide/ferricyanide ($Fe(CN)_6^{4-}/Fe(CN)_6^{3-}$, at 10 mmol L^{-1}), having KCl (50.0 mmol L^{-1}) as the supporting electrolyte. All electrodes were made from platinum-based wire (0.50 mm diameter). Scan rate: 50 mV s^{-1} and step potential: 2.5 mV.

cates the reversibility of the redox probe under the experimental conditions. The observed ohmic drop, evidenced by the increased peak-to-peak separation,[29] can be attributed to both the geometric configuration of the electrochemical cell and the specific arrangement of the electrodes within the dual-compartment setup. Notably, the isolation of the PRE within an external compartment, which prevents direct ionic contact with the analyte stream flowing past the WE and CE, is likely a major contributor to the observed ohmic resistance. Furthermore, the characteristic shape of the voltammogram (Fig. 2 and Fig. S2, SI) demonstrates a wide operational potential window, confirming the proper functionality and activity of the electrode array (WE and CE) integrated on the flowing stream channel.

The typical well-defined voltammetric profiles and the wide operational potential window (>1.8 V, Fig. 2) qualitatively resemble those obtained by conventional electrodes arranged in conventional electrochemical cells. This behavior, observed despite the PRE's external positioning, supports its effectiveness in controlling the WE's potential. The lack of direct ionic contact with the flowing stream within the channel minimizes any potential interference from the sample matrix or its electrochemical products on the PRE's potential. This isolation ensures that the PRE maintains a stable and well-defined potential, against which the working electrode's potential is accurately measured and controlled by the potentiostat. As a result, any changes observed in the electrochemical signal at the WE can be confidently attributed to the analyte's redox behavior under the applied potential, rather than to fluctuations or drift in the PRE's potential caused by direct interaction with the flowing solution within the PDMS-based electroanalytical platform. The demonstrated performance supports the applicability of this device for quantifying electroactive species at sample-relevant concentrations *via* voltammetric and amperometric techniques.

3.2. Chronoamperometric study using an air-driven carrier

A typical three-electrode configuration is frequently used in flow injection electroanalysis.[30–33] However, a significant operational concern with this configuration is the accidental occurrence of air bubbles, which can cause considerable damage to the WE by creating conditions of extreme electrochemical potential.[19] Consequently, when this happens, the experiments should be stopped, and the flow cell disassembled because the WE requires physical polishing to regenerate its active surface. The intricate geometries present in these flow cells introduce extensive overhead time during crucial polishing and rinsing/washing procedures. While more prevalent among less experienced users, this issue is mitigated with practice, developing the necessary skills to prevent air bubble formation.[19] However, this inherent time consumption poses a growing challenge, as modern analytical methods increasingly prioritize rapid analysis and adherence to green chemistry principles. In turn, this extended processing time reduces the system's practicality.[19]

Addressing this inherent challenge, we developed a flow cell with a dual-detection system that maintains accurate peak current measurements even with the deliberate introduction of air into the carrier solution.[17–19,27,28] This reliable performance arises from the flow cell's design, which allows for effective potential control of the WE within the upper reservoir. Consequently, we now turn our attention to an investigation into the feasibility of using air as a carrier to drive the analyte/sample through the channel towards the integrated electrode array within the flowing stream. The subsequent sections will detail the design and operation of our proposed PDMS-based electroanalytical platform, emphasizing its performance characteristics and potential applications in electroanalysis.

The resulting chronoamperogram for the air-driven carrier $Fe(CN)_6^{4-}/Fe(CN)_6^{3-}$ (1.00 mmol L^{-1}) solution (Fig. 3a, without smoothing signal) showed high, narrow, and slightly noisy peaks. However, these characteristics did not hamper the clear identification of peak currents following six discrete injections (10 µL), suggesting an enhanced flux of electroactive species to the electrode surface and a faster electron transfer rate. Applying appropriate smoothing to the signal for noise reduction (Fig. 3b) effectively eliminated variations unrelated to the analyte's redox reactions, enabling a more accurate interpretation of the peak current. The average peak current of 0.97 ± 0.14 µA indicates the effective application of the air-driven flow system for achieving precise and reproducible results, particularly valuable in quantitative analyses. In addition, the use of signal smoothing for noise reduction enhanced the electrochemical system's detection limits and improved measurement accuracy by effectively separating the analyte's response from the background current.[19]

The integration of the electrodes into two distinct configurations—notably keeping the PRE in a separate reservoir—

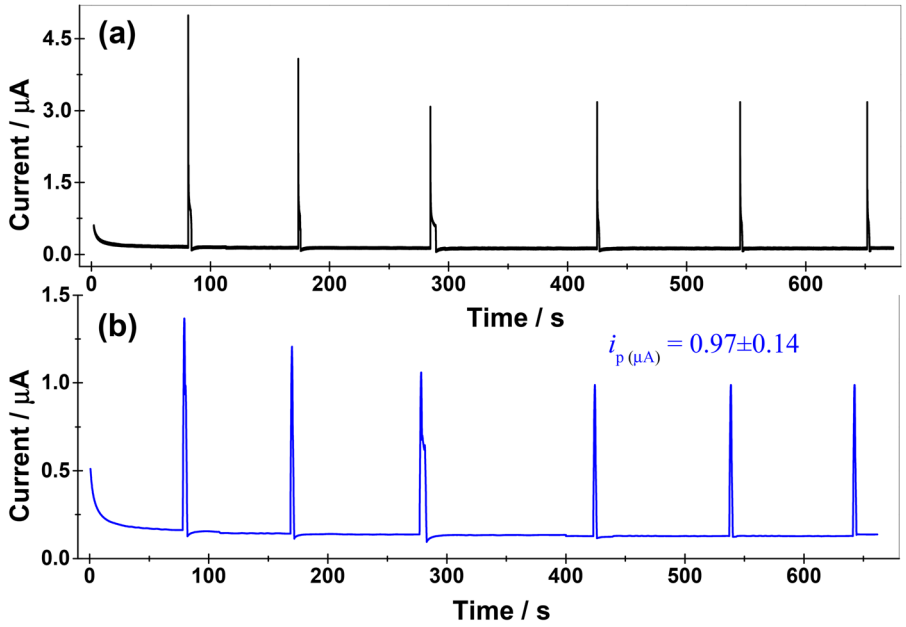

Fig. 3 Chronoamperograms recorded for discrete injections (10 μL) of $Fe(CN)_6^{4-}/Fe(CN)_6^{3-}$ (1.00 mmol L^{-1}, in a 50.0 mmol L^{-1} KCl solution) for comparing the performance of the proposed electrochemical system in the absence (a) and presence (b) of signal smoothing for noise reduction. Conditions: applied potential 0.60 V and flow rate of 1.00 μL s^{-1}. All electrodes were made from platinum-based wire (0.50 mm diameter).

ensures accurate peak current measurements, even under challenging conditions like an air-driven system. Unlike traditional liquid-flow systems, where peak shapes are often distorted by sample dispersion along the channel, our approach minimizes analyte dilution due to the limited interaction with the air carrier, resulting in high system performance (Video S1). Moreover, we employed a spiral-shaped channel design to reduce any extra flow disturbances during discrete analyte/sample injection using an automated micropipette. This specific geometry facilitates smoother sample introduction, reducing potential noise from unexpected system variations. Likewise, precise control of the airflow within the channel, achieved *via* the syringe pump, was crucial for consistently driving the injected analyte solution and ensuring uniform conditions throughout all experiments.

A full factorial experimental design (2^3) systematically evaluated the concurrent effects of multiple independent variables: analyte/sample injection volume (controlled to maintain flow consistency), airflow rate (adjusted to guarantee the fluidity of the analyte along the channel) and applied detection potential (which can be optimized to improve the sensitivity and precision of the measurements). These three factors varied across two levels, resulting in eight experimental combinations (Exp 1 to Exp 8, Table S1, SI) that revealed interaction effects impacting system performance and peak current measurement. Fig. S3A (SI) shows that the effectiveness of the analyte discrete injection volume depended on both the airflow rate and applied potential. Experiment 6, using an injection volume of 10 μL, an airflow rate of 1.00 μL s^{-1}, and an applied potential of 0.60 V (Fig. S3B, SI), generated a more Gaussian-like shape and symmetry with maximum current intensity. The enhanced peak current under these conditions, using an air-driven flow system, can be attributed to the minimized dispersion during transport from the injector to the electrode array.[19]

High injection volumes can overload the system, altering the channel hydrodynamics and resulting in broad or asymmetric peaks due to the prolonged residence time of the analyte on the electrodes. In contrast, insufficient volumes compromise analytical sensitivity, limiting detection efficiency. Likewise, excessive airflow rates induce turbulence, impairing the homogeneity of the contact between the analyte and the electrodes, while reduced flows increase the residence time, intensifying undesirable effects such as diffusion and signal misrepresentation. Additionally, poorly adjusted detection potentials underestimate the oxidation/reduction processes of the analyte, reducing peak intensity. In this context, optimizations based on response surfaces allow identifying operational windows that maximize the faradaic current. Thus, variables such as flow rate and injection volume directly influence the adhesion of the analyte to the electrode surface, while the detection potential modulates the electrochemical polarization. The analysis of individual and interactive effects revealed dominant variables, such as detection potential, and second-order interactions between flow rate and volume, highlighting the need for multivariate approaches for integral system optimization.

While the proposed device showed acceptable repeatability, some inconsistencies in peak current intensity and shape were observed. This variability was attributed to the rapid transport of larger sample volumes—nearly filling the inter-electrode space—and the apparent tendency of the PDMS material to form an irregular film along the channel walls. Using a 10 μL

injection volume ensured sufficient analyte distribution across the electrodes within the flow-through cell compartment, enabling efficient electrical contact and effective charge transfer. An airflow rate of 1.00 μL s^{-1} also optimized mass transport to the electrode surface while minimizing dispersion of the analyte in the injected aliquot. The applied potential was important for enhancing analyte oxidation; however, potentials higher than 0.65 V can induce undesirable secondary reactions that compromise the peak current measurement.

The chronoamperometric measurements (Fig. S4, SI) revealed a slight dependence of the peak current on the B–R buffer concentrations (10.0 and 40.0 mmol L^{-1} in the presence of KCl at 50.0 mmol L^{-1}), indicating that buffer concentration likely affects peak current, possibly by hindering salicylic acid mass transport due to a reduced diffusion coefficient. Further insights are provided by the pH-dependent behavior, which illustrates the significant oscillation of the peak oxidation current of salicylic acid across a range of pH values (as shown in Fig. S5A). Notably, within the near-neutral pH range of 5.0 to 7.0, salicylic acid exhibited the maximum current signal, which also presented a more symmetrical peak shape. This observation suggests that within this pH range, salicylic acid is likely present in its electroactive form, enabling more efficient electron transfer at the electrode surface. Chronoamperometric analysis (Fig. S5B) also reveals negligible electrochemical activity (residual current) upon discrete injection of the supporting electrolyte (Fig. S5, BI). Subsequent injection of salicylic acid (prepared in the supporting electrolyte) resulted in a distinct peak current (Fig. S5, BII), confirming its electroactive nature through effective analyte–electrode interaction and enhanced charge-transfer kinetics at the electrode surface.

3.3. Comparative study of air-driven *vs.* liquid-driven electroanalysis

As previously demonstrated in liquid-flow electroanalysis, maintaining a consistent flow without disrupting fluid mechanics and electrochemical measurements in the presence of air bubbles presents a significant challenge.[17–19,27,28] Here, to mitigate such malfunctions, the liquid-flow electroanalysis was performed by carefully pumping the supporting electrolyte solution through the channel to ensure a uniform and bubble-free flow. Using identical experimental parameters, we conducted studies to compare the performances of the device in detecting salicylic acid (1.00 mmol L^{-1}) in spiked aqueous samples (river water, groundwater, and lake water) when using either an air-driven or a liquid-driven carrier (Fig. 4).

Chronoamperograms obtained after four discrete injections, using either continuous liquid-flow or airflow as the carrier, show that the designed dual-mode electrochemical detection works properly under both conditions. Across all spiked samples, the air-driven system consistently yielded the highest and most well-defined peak currents. This signal enhancement is likely due to minimal analyte dilution during its transport from the injector to the electrodes.[19] Furthermore, we reiterate that the configured dual-mode electrochemical detection effectively reduces noise and turbulence associated with micropipette discrete injection and minimizes potential drops caused by bubbles.

Beyond the minimum analyte dilution along the channel, we can assume a unidirectional flow in a non-reactive system operating under laminar convection-diffusion conditions, on which the mass transport of analytes toward the WE can be studied using eqn (1):[34,35]

$$\frac{dC_i}{dt} = \frac{D_{ij}\partial^2 C_i}{\partial z^2} - \frac{\vec{v}\partial C_i}{\partial z} \quad (1)$$

where C_i denotes the concentration of species i, D_{ij} is the diffusion coefficient of species i in medium j and $\vec{v}$ is the flow velocity vector.

Under the optimized airflow conditions, we estimate that mass transport occurs predominantly in the diffusive regime, where the analyte flux is primarily governed by the D_{ij} coefficient. Notably, D_{ij} exhibits substantially higher values in the gas phase, thereby enhancing diffusion-driven analyte transport towards the WE and facilitating its detection compared to aqueous systems.

Earlier, we highlighted the need for integrating stable reference/pseudo-reference electrodes (RE/PRE) for accurate potential measurements in miniaturized, fully integrated flow-based electrochemical platforms utilizing a standard three-electrode configuration.[17–19,27,28] Although these electrodes are often placed in direct contact with the flowing solution in microfluidic systems,[36–39] this arrangement can compromise potential control if laminar flow is not maintained.[19] Under non-ideal flow conditions, issues such as bubble formation can lead to potential drops by reducing the electrochemically active surface area (EASA) or through electrode fouling caused by adsorbed electrogenerated products, thus hindering their proper function.[17,19,27,28,40,41] Similarly, pulsations from pumping systems can be detected by both the WE and RE/PRE, leading to an abrupt potential fluctuation at the interface and introducing significant noise that directly impacts the electrochemical response.[18]

The series of chronoamperograms shown in Fig. 5 and S6 (SI) illustrates the viability of the proposed electrochemical device featuring two distinct electrode arrangements within the microfluidic channel. The first one placed a downstream two-electrode setup where the CE and PRE are linked *via* a single potentiostat cable (Fig. 5, I and III, also Fig. S6-SI), and a three-electrode configuration based on the earlier design (Fig. 5, II and IV, also Fig. S6-SI). The two-electrode configuration (detailed in Fig. 5, I and III, also Fig. S6-SI) was initially investigated due to its common use and its ability to locate the CE downstream of the WE or at the channel's terminal, thereby minimizing the interference caused by the leakage current to the PRE.[42,43] Comparing liquid-driven and air-driven carriers for analyte transport showed that the liquid-driven approach yielded highly reproducible peak current intensities. Conversely, the air-driven system resulted in an increased peak current in all studied spiked aqueous samples (Fig. 5 and S6-SI), likely because it minimized analyte dilution during its transport from the injector to the detection region.

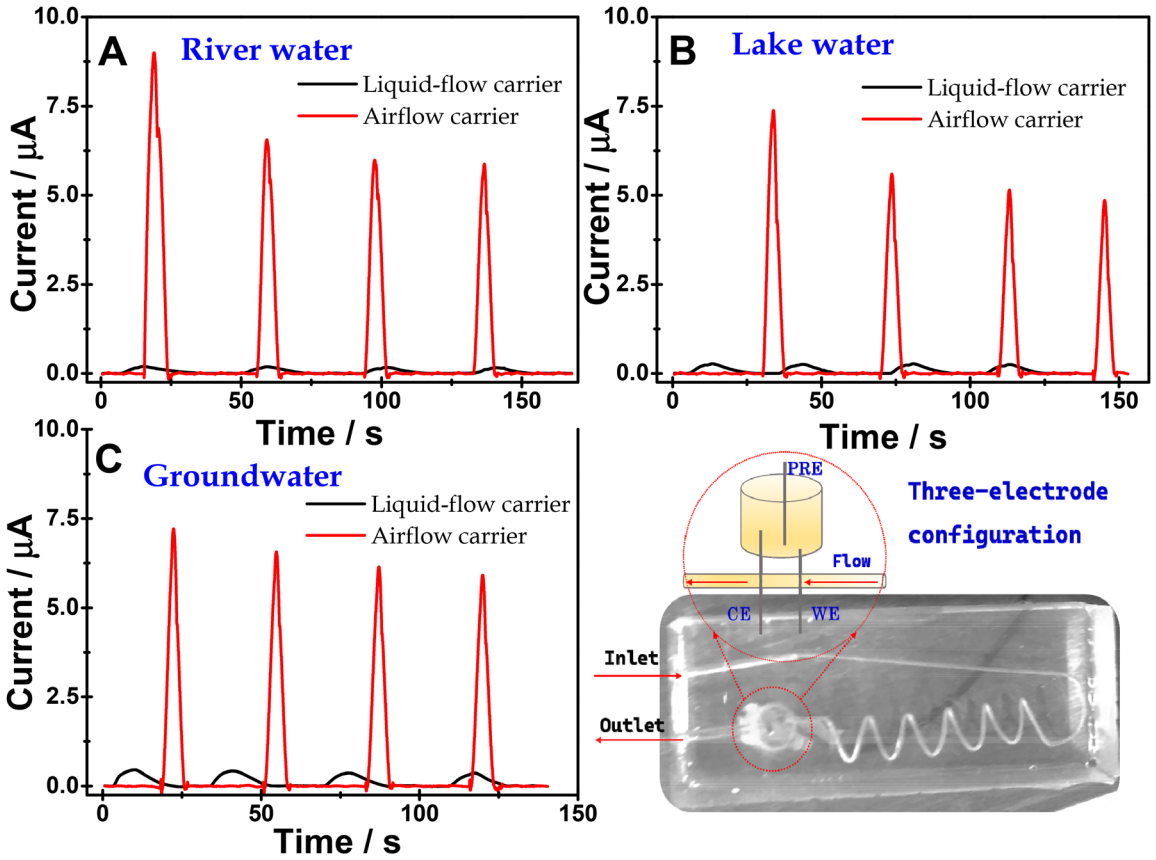

Fig. 4 Chronoamperograms, after smoothing the signal for noise reduction, recorded to compare liquid-driven and air-driven systems used to carry discrete analyte injection into the microfluidic system. Analyte: salicylic acid at 1.00 mmol L^{-1} prepared in a B–R buffer solution (10.0 mmol L^{-1} at pH 7.0) containing KCl (50.0 mmol L^{-1}) to adjust the ionic strength. The liquid-flow carrier was a B–R buffer (10.0 mmol L^{-1} at pH 7.0) containing KCl (50.0 mmol L^{-1}) to adjust the ionic strength. Fixed flow parameters: a flow rate of 15 μL s^{-1}, an injection volume of 100 μL, and an applied potential of 0.60 V were used.

Positioning the PRE outside the flow channel essentially establishes electrical communication between the WE and CE without direct exposure to the channel's internal fluid dynamics. This external configuration can enhance stability by minimizing disruptions from fluid flow or contaminants originating from electrogenerated products or the sample itself within the channel, generating more accurate peaks even in different spiked real-world samples (Fig. 5 and S6-SI). In contrast, placing the PRE in direct contact with the flowing stream (Fig. 5, I and III) increases its susceptibility to disturbances caused by fluid dynamics, contamination, or variations in ionic strength, which can compromise signal intensity and measurement reliability.[17–19,27,28] Overall, locating the PRE outside the flow-based channel improved its operational stability by isolating it from the channel's fluid dynamics and potential contaminants (Fig. 5, II and IV). Moreover, using an air-driven flow system can further assist in reducing interference and optimizing signal quality.

3.4. Proof-of-concept application

Firstly, optimization of the liquid-flow carrier parameters was conducted using a factorial design 2^3 (details in Table 2, SI; Fig. S7, SI), revealing that the effectiveness of a specific analyte injection volume is strongly dependent on the flow rate. Experiment 8 yielded the highest current intensity with a 100 μL injection volume, a 15 μL s^{-1} flow rate, and an applied potential of 0.60 V. This specific combination of flow rate and injection volume (15 μL s^{-1} and 100 μL, respectively) was determined to optimize mass transport to the WE surface. Injection volumes lower than 50.0 μL resulted in undetectable signals, likely due to dilution of salicylic acid within the liquid-flow carrier.

The analytical performance comparing both airflow and liquid-flow carriers (Table S3, SI) demonstrated the proper operation under both conditions for detecting $Fe(CN)_6^{4-}$/$Fe(CN)_6^{3-}$ and salicylic acid within the same concentration ranges. Both systems exhibited reliable linear responses with high coefficients of determination (R^2), indicating a strong correlation between analyte concentration and detected signal. Notably, salicylic acid electroanalysis exhibited slightly superior linearity and a lower detection limit compared to the redox probe. These results indicate that the proposed device can detect salicylic acid at a lower detection limit (Table S3, SI) while maintaining accurate detection within the specified range.

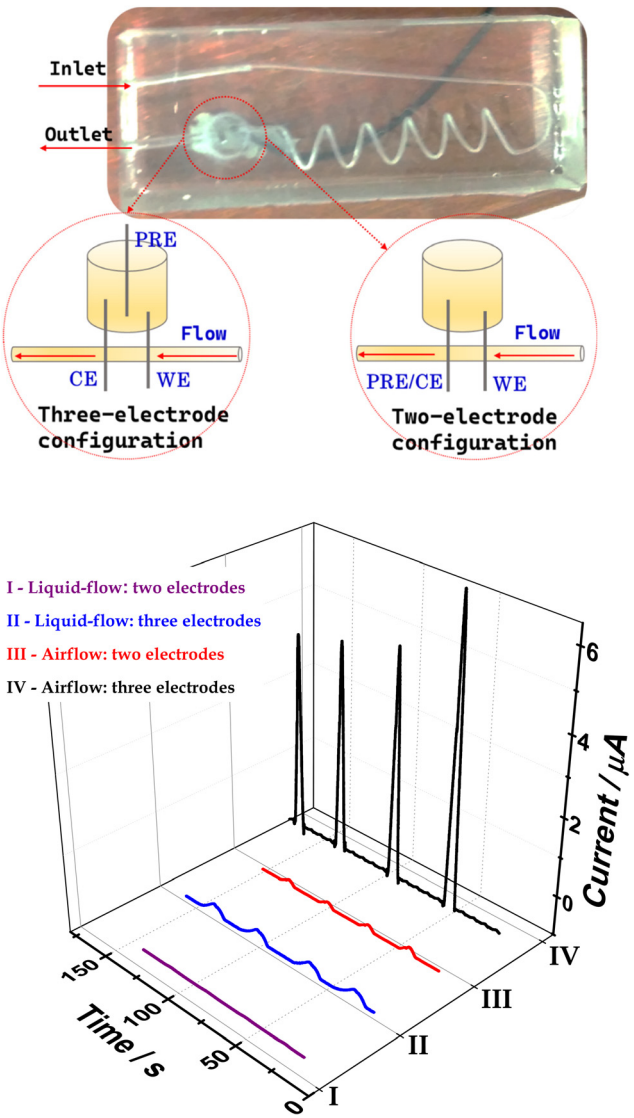

Fig. 5 Chronoamperograms, after smoothing the signal for noise reduction, registered to compare the electrochemical performance of the device holding two (I and III) and three (II and IV) electrode configurations using liquid-flow and airflow carriers. Parameters: a flow rate of 15 μL s^{-1}, an injection volume of 100 μL, and an applied potential of 0.60 V. Salicylic acid (at 1.00 mmol L^{-1}) was diluted in a B–R buffer (10.0 mmol L^{-1} at pH 7.0) containing KCl (50.0 mmol L^{-1}) to adjust the ionic strength. The prepared electrolytic solution was made from a groundwater sample. The liquid-flow carrier was a B–R buffer (10.0 mmol L^{-1}) at pH 7.0, with the ionic strength adjusted using KCl (50.0 mmol L^{-1}).

To validate the proposed device, its performance using an air-driven carrier was evaluated and compared with that of a similar experiment employing a liquid-flow carrier for the quantification of salicylic acid (1.00 mmol L^{-1}) in spiked aqueous samples (Table 1). The measured concentrations of salicylic acid showed acceptable agreement with the spiked (claimed) values, yielding recovery values consistently above 85% for both methods across all tested matrices. Notably, an increasing trend in recovery values was observed in river water

Table 1 Repetitive addition–recovery experiments were carried out to evaluate the quality of the data obtained in the determination of salicylic acid in spiked aqueous samples using an airflow carrier (optimized conditions of flow rate: 1.00 μL s^{-1}, potential: 0.60 V and injection volume: 10 μL) and a liquid-flow carrier (optimized conditions of flow rate: 15 μL s^{-1}, potential: 0.60 V and injection volume: 100 μL)

Carrier	Sample	Spiked/ mmol L^{-1}	Found ± μ/ mmol L^{-1}	Recovery (%)
Airflow	River water	1.00	1.12 ± 0.3	112
	Lake water	1.00	0.94 ± 0.2	94.0
	Groundwater	1.00	0.99 ± 0.2	99.0
Liquid-flow	River water	1.00	0.89 ± 0.1	89.0
	Lake water	1.00	0.85 ± 0.1	85.0
	Groundwater	1.00	1.50 ± 0.2	150

(air-driven carrier) and groundwater (liquid-flow carrier) samples, which may be attributed to progressive electrode fouling—where sample constituents accumulate on the electrode surface over time. This interference may have led to signal amplification, resulting in apparently higher-than-expected recovery values.

Applying airflow as a carrier for salicylic acid detection offers several benefits compared to conventional liquid-flow systems. A key advantage is the reduced risk of WE contamination typically associated with aqueous solution carriers, thereby minimizing potential interferences that could impair analytical accuracy. Furthermore, using airflow as a carrier reduces maintenance demands due to a lower tendency for channel clogging, a common issue in liquid-based carriers. The naturally high flow velocity of air promotes efficient analyte transport virtually without any dilution. Air-based systems also avoid troubles related to bubble formation, which can disturb liquid flow and compromise measurements. Additionally, they facilitate the effective use of small sample volumes without substantial analyte dilution within the channel.[44]

Despite these advantages, precise airflow control presents a challenge that requires attention during method development. Fluctuations in airflow can lead to variations in analyte delivery rates, potentially affecting measurement accuracy by causing minor signal intensity differences. However, despite challenges in precise flow control and the potential for injection-induced perturbations, air-driven systems demonstrate high performance in terms of green chemistry metrics, reduced dilution, and robustness against bubble interference, making them a promising alternative to conventional liquid-driven methods.

3.5. Ecological impact

The principles of Green Analytical Chemistry guided the development of a more sustainable and environmentally friendly analytical system. The ecological profile of the electroanalytical method using our proposed device was assessed using the AGREE metric, with equal weighting applied to all 12 evaluation criteria (detailed scores in Table S4, SI). Notably, the air-driven method demonstrated superior ecological performance

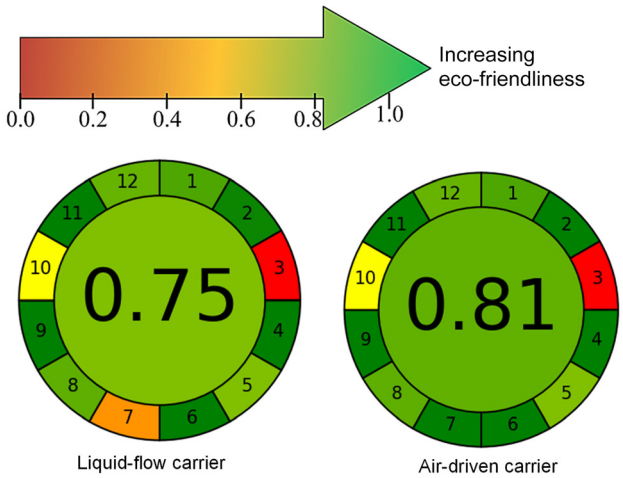

Fig. 6 Color scale corresponds to the reference and results of the AGREE analysis used to assess the ecological impact of the air-driven carrier compared with the liquid-flow carrier during electroanalysis development. The details of the evaluated scores assigned to each criterion are presented in Table S4 (SI).

compared to the liquid-flow method (Fig. 6), achieving higher AGREE scores for variables related to quantitative analysis and waste generation. This advantage arises from the air-driven system's smaller sample injection volume, leading to less waste. In contrast, the conventional liquid-flow method, with its continuous pumping of a liquid mobile phase, requires larger injection volumes with more significant waste generation.

Both methods achieved the same favorable scores for eliminating sample preparation steps and for their high energy efficiency (0.080 kWh), as analyses required only a potentiostat connected to a laptop and a syringe pump. The incorporation of some reagents derived from renewable sources, along with the exclusion of toxic reagents or solvents, further enhanced the environmental compatibility of our proposed method. Beyond its sustainable aspects, the method is designed for practical application while ensuring reliable and reproducible measurements. Although the air-driven method received lower AGREE scores for principles 3 and 10 (Fig. 6), its overall ecological impact remained high.

While the numerical difference of 0.6-points (Fig. 6) might seem negligible at first sight, it can be highlighted that this specific increment represents a substantial improvement within the context of AGREE analysis, especially when considering the inherent limitations and common scoring patterns in this type of assessment. Given the inherently green nature of miniaturized electroanalytical systems, any further improvement is a testament to major innovation. Herein, the target interpretation can be based on critical factors such as considerable progress in advancing the green chemistry profile of the proposed method for criteria 2 and 7 (sample quantity and residues), respectively (Table S4, SI). AGREE analysis evaluates various green metrics, and achieving even a modest numerical gain often requires substantial innovations or optimizations in multiple steps, such as reduced waste, lower energy consumption, or safer reagent use. Thus, such a gain directly reflects a major step forward to enhance the sustainability of the proposed electroanalytical approach and achieve a green process.

4. Conclusion

The innovative design offers considerable advancements for electroanalysis in flow systems. The proposed system ensures very reproducible transient signals, enabling accurate and reliable measurements even when dealing with air bubble formation or complex real-world samples on the electrode surface. Using the proposed air-driven system to replace the traditional liquid-flow in electroanalytical applications yields several benefits: (I) elimination of the preparation and storage of large volumes of supporting electrolyte solutions, thereby lowering costs and the potential for contamination or interference from undesirable constituents; (II) reduction in reagent consumption and waste generation, aligning with green and sustainable practices; (III) potentiality for the electroanalysis of analytes that are unstable or insoluble in aqueous or organic carriers, increasing the range of applications; (IV) opportunities for enhanced sensitivity due to improved mass transport resulting from the absence of dilution inside tubes and channels; and (V) preventing channel clogging, which is a common issue in flow-through electroanalysis.

Beyond these technical benefits, the proposed system aligns with sustainability principles and Green Analytical Chemistry, besides lowering operational costs by enabling the use of smaller solution volumes. This configuration represents a notable step forward, integrating efficiency with more environmentally friendly electroanalysis, making it a valuable tool for applications requiring minimal sample volumes and cost-effective testing evaluations.

Author contributions

The manuscript was written through the contributions of all authors. All authors have approved the final version.

Conflicts of interest

The authors declare no competing financial interest.

Data availability

This work did not generate any new data. All relevant data are included within the manuscript and its SI.

SI includes: histograms showing measurement distribution for the channel, cyclic staircase voltammograms recorded at various scan rates, factorial design applied for experimental optimization along with the corresponding chronoampero-

grams, comparisons of electrochemical performance using two and three electrode configurations with liquid-flow and airflow carriers, and analytical parameters derived from calibration curves that assess the performance of both systems. See DOI: https://doi.org/10.1039/d5gc02382c.

Acknowledgements

The authors gratefully acknowledge the financial support provided by the Brazilian funding agency CNPq (Grant: 444379/2024-0 and 310827/2021-3), CNPq/INCT (Grant: 465571/2014-0), and FINEP (contract: 04.13.0448.00/2013). T. S. B. de Barros is especially grateful for the scholarship awarded by the CAPES program.

References

1 M. Trojanowicz and K. Kołacińska, *Analyst*, 2016, **141**, 2085–2139.
2 J. (Jarda) Ruzicka and P. Chocholouš, *Talanta*, 2024, **269**, 125410.
3 M. Trojanowicz, *Advances in flow analysis*, John Wiley & Sons, 2008.
4 K. Tóth, K. Stulik, W. Kutner, Z. Fehér and E. Lindner, *Pure Appl. Chem.*, 2004, **76**, 1119–1138.
5 H. A. J. Al Lawati, *Luminescence*, 2013, **28**, 618–627.
6 S. Kurbanoglu, M. A. Unal and S. A. Ozkan, *Electrochim. Acta*, 2018, **287**, 135–148.
7 G. M. Whitesides, *Nature*, 2006, **442**, 368.
8 M. Trojanowicz and K. Kołacińska, *Analyst*, 2016, **141**, 2085–2139.
9 R. H. Liu, R. Lenigk, R. L. Druyor-Sanchez, J. Yang and P. Grodzinski, *Anal. Chem.*, 2003, **75**, 1911–1917.
10 D. Ahmed, C. Y. Chan, S.-C. S. Lin, H. S. Muddana, N. Nama, S. J. Benkovic and T. Jun Huang, *Lab Chip*, 2013, **13**, 328–331.
11 Y. Gao, M. Wu, Y. Lin, W. Zhao and J. Xu, *Microfluid. Nanofluid.*, 2020, **24**, 29.
12 Y. Li, X. Liu, Q. Huang, A. T. Ohta and T. Arai, *Lab Chip*, 2021, **21**, 1016–1035.
13 P. K. Dasgupta and S. Liu, *Anal. Chem.*, 1994, **66**, 1792–1798.
14 J. D. Stucki and O. T. Guenat, *Lab Chip*, 2015, **15**, 4393–4397.
15 K. Khoshmanesh, A. Almansouri, H. Albloushi, P. Yi, R. Soffe and K. Kalantar-zadeh, *Sci. Rep.*, 2015, **5**, 9942.
16 X. Zhao, C. Ma, D. S. Park, S. A. Soper and M. C. Murphy, *Sens. Actuators, B*, 2022, **361**, 131687.
17 E. M. Maximiano, T. Sequinel, C. A. Martins, L. Angnes and M. A. Gonçalves Trindade, *Talanta*, 2021, **221**, 121611.
18 M. A. G. Trindade, C. A. Martins, L. Angnes, T. Herl, T. Raith and F. M. Matysik, *Anal. Chem.*, 2018, **90**, 10917–10926.
19 L. H. de Oliveira, M. A. G. Trindade and L. Angnes, *Talanta*, 2025, **281**, 126875.
20 X. Zhao, H. Ren and L. Luo, *Langmuir*, 2019, **35**, 5392–5408.
21 H. Vogt, *J. Appl. Electrochem.*, 1983, **13**, 87–88.
22 A. Raman, P. Peñas, D. van der Meer, D. Lohse, H. Gardeniers and D. Fernández Rivas, *Electrochim. Acta*, 2022, **425**, 140691.
23 Ç. Demirkır, J. A. Wood, D. Lohse and D. Krug, *Langmuir*, 2024, **40**, 20474–20484.
24 A. Angulo, P. van der Linde, H. Gardeniers, M. Modestino and D. Fernández Rivas, *Joule*, 2020, **4**, 555–579.
25 M. Regnier, C. Vega, D. I. Ioannou and T. Noël, *Chem. Soc. Rev.*, 2024, **53**, 10741–10760.
26 J. R. Lake, Á. M. Soto and K. K. Varanasi, *Langmuir*, 2022, **38**, 3276–3283.
27 E. M. Maximiano, D. A. Gonçalves, C. A. Martins, L. Angnes, R. S. Gomes and M. A. G. Trindade, *Talanta*, 2021, **233**, 122514.
28 J. da Silva do Carmo, L. M. Roveda, R. Rodrigues, C. T. de Carvalho and M. A. G. Trindade, *Electroanalysis*, 2024, **36**, e202300382.
29 V. B. Messias, D. C. P. Modenez, C. E. de Souza Pereira, R. M. Takeuchi and A. L. dos Santos, *Electrochim. Acta*, 2025, **511**, 145374.
30 F. S. Felix and L. Angnes, Elsevier, 2010, preprint, DOI: 10.1002/jps.22192.
31 F. Silva Felix, L. Angnes, A. Escarpa, M. C. González and M. Á. López, in *Agricultural and Food Electroanalysis*, John Wiley & Sons, Ltd, 2015, pp. 49–72.
32 J. R. C. Da Rocha, L. Angnes, M. Bertotti, K. Araki and H. E. Toma, *Anal. Chim. Acta*, 2002, **452**, 23–28.
33 M. A. Franco, D. A. G. Araújo, L. H. Oliveira, M. A. G. Trindade, R. M. Takeuchi and A. L. Santos, *Anal. Methods*, 2016, **8**, 8420–8426.
34 T. Gervais and K. F. Jensen, *Chem. Eng. Sci.*, 2006, **61**, 1102–1121.
35 Y. Ma, C. Sella and L. Thouin, *Anal. Chem.*, 2024, **96**, 14650–14659.
36 D. Agustini, M. F. Bergamini and L. H. Marcolino-Junior, *Lab Chip*, 2016, **16**, 345–352.
37 J. L. Erkal, A. Selimovic, B. C. Gross, S. Y. Lockwood, E. L. Walton, S. McNamara, R. S. Martin and D. M. Spence, *Lab Chip*, 2014, **14**, 2023–2032.
38 F. Sassa, G. C. Biswas and H. Suzuki, *Lab Chip*, 2020, **20**, 1358–1389.
39 R. D. Sochol, E. Sweet, C. C. Glick, S. Y. Wu, C. Yang, M. Restaino and L. Lin, Elsevier, 2018, preprint,DOI: 10.1016/j.mee.2017.12.010.
40 K. Tóth, K. Stulik, W. Kutner, Z. Fehér and E. Lindner, *Pure Appl. Chem.*, 2004, **76**, 1119–1138.
41 B. J. Polk, A. Stelzenmuller, G. Mijares, W. MacCrehan and M. Gaitan, *Sens. Actuators, B*, 2006, **114**, 239–247.
42 T. Li, J. A. Díaz-Real and T. Holm, *Adv. Mater. Technol.*, 2021, **6**, 2100569.
43 T. Li, J. A. Díaz-Real and T. Holm, *ACS Sens.*, 2022, **7**, 2934–2939.
44 Y. Song, X. Zhao, Q. Tian and H. Liang, *2 Fundamental Concepts and Physics in Microfluidics*, 2018.